Title

A short HLA-DRA isoform binds the HLA-DR2 heterodimer on the outer domain of the peptide-binding site.

Authors

Shams, Hengameh
Hollenbach, Jill A
Matsunaga, Atsuko
et al.

Publication Date

2022-04-01

DOI

10.1016/j.abb.2022.109156

Peer reviewed

HHS Public Access

Author manuscript

Arch Biochem Biophys. Author manuscript; available in PMC 2023 April 15.

Published in final edited form as:

Arch Biochem Biophys. 2022 April 15; 719: 109156. doi:10.1016/j.abb.2022.109156.

A short HLA-DRA isoform binds the HLA-DR2 heterodimer on the outer domain of the peptide-binding site

Hengameh Shams[1], **Jill A. Hollenbach**[1,2], **Atsuko Matsunaga**[1], **Mohammad R. K. Mofrad**[3], **Jorge R. Oksenberg**[1], **Alessandro Didonna**[1,4,*]

[1]Weill Institute for Neurosciences, Department of Neurology, University of California, San Francisco, CA 94158, USA

[2]Department of Epidemiology and Biostatistics, University of California, San Francisco, CA 94158, USA

[3]Departments of Bioengineering and Mechanical Engineering, University of California, Berkeley, CA 94720, USA

[4]Department of Anatomy and Cell Biology, East Carolina University, Greenville, NC 27834, USA

Abstract

The human leukocyte antigen (*HLA*) locus encodes a large group of proteins governing adaptive and innate immune responses. Among them, HLA class II proteins form α/β heterodimers on the membrane of professional antigen-presenting cells (APCs), where they display both, self and pathogen-derived exogenous antigens to CD4+ T lymphocytes. We have previously shown that a shorter HLA-DRA isoform (sHLA-DRA) lacking 25 amino acids can be presented onto the cell membrane via binding to canonical HLA-DR2 heterodimers. Here, we employed atomistic molecular dynamics simulations to decipher the binding position of sHLA-DRA and its structural impact on functional regions of the HLA-DR2 molecule. We show that a loop region exposed only in the short isoform (residues R69 to G83) is responsible for binding to the outer domain of the HLA-DR2 peptide-binding site, and experimentally validated the critical role of F76 in mediating such interaction. Additionally, sHLA-DRA allosterically modifies the peptide-binding pocket conformation. In summary, this study unravels key molecular mechanisms underlying sHLA-DRA function, providing important insights into the role of full-length proteins in structural modulation of HLA class II receptors.

[*]Corresponding Author: Department of Anatomy and Cell Biology, Brody School of Medicine, East Carolina University, 600 Moye Boulevard, Greenville, NC 27834, Tel: +1 252 744 1854, didonnaal21@ecu.edu.

Author contributions

AD, HS, JRO, and JH conceived and supervised the project. HS conducted all the molecular dynamics simulations. AD and AM carried out the biological assays. HS, AM, and AD analyzed the data. HS, MRK, JH, JRO and AD wrote the paper. All authors read and approved the final manuscript.

Conflict of interest

The authors declare no competing interests. All the data supporting the findings of this study are available from the corresponding author upon reasonable request.

Graphical Abstract

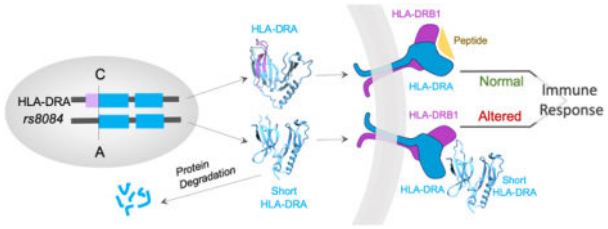

Keywords

Antigen Presentation; Molecular Dynamics; Protein-Protein Binding; Structural Modulation

Introduction

Human leukocyte antigen (HLA) molecules are conserved glycoproteins that expose antigens on the cell surface for T cell recognition in the context of adaptive and innate immunity [1,2]. Class I HLA proteins are expressed by all nucleated cells and present antigens of endogenous nature to cytotoxic $CD8^+$ T lymphocytes. Conversely, class II HLA proteins principally present exogenous antigens to helper $CD4^+$ T lymphocytes and their expression is restricted to professional antigen presenting cells (APCs) such as B lymphocytes, dendritic cells, and macrophages [2].

From a structural standpoint, both classes of molecules are constituted by two non-covalently associated chains (α/β) forming heterodimers with an extracellular portion, a transmembrane region, and a cytoplasmic tail [3–5]. A groove in the extracellular domain functions as a binding pocket in which the peptidic antigen is accommodated and stabilized through hydrogen bonds and ion bridges between residues inside the cleft and the antigen [4]. Peptides ranging between 13 and 25 residues, products of the intracellular antigen degradation process constitute the typical antigen repertoire of class II molecules, while only peptides with 8 to 10 residues can fit into the class I pockets [6]. Interestingly, while the class I HLA pocket is closed at both ends, the binding site of class II HLA molecules is open allowing more flexibility in the repertoire of antigens that can be displayed [4,7]. Furthermore, the N and C termini of antigens do not directly interact with the class II groove and may extend beyond the ends of the pocket, allowing in some cases full-length proteins to be efficiently presented without being processed to peptides. A partially folded form of the hen egg white lysozyme (*HEL) was the first example reported of such intact antigens [8]. Subsequently, bovine RNAse and horse myoglobin were shown to interact with HLA class II molecules in their full-length forms [7]. Furthermore, misfolded endogenous proteins including the class I allele HLA-Cw4 and IgG heavy chains have been characterized as additional proteolytic-independent HLA class II substrates [9].

We have recently reported that an isoform of class II α-chain (HLA-DRA) functions as a novel intact antigen for class II heterodimers [10]. Specifically, we demonstrated that a splice acceptor variant (rs8084) in the *HLA-DRA* gene drives the expression of an alternative form of HLA-DRA lacking 25 amino acids in its extracellular domain. rs8084

is in full linkage disequilibrium with *HLA-DRB1*15:01*, a common allele in European populations [10]. The alternative splicing promoted by the *A* allele of rs8084 is a stochastic event, thus both short and standard α-chains are expressed in APCs of *A* carriers. The shorter isoform (sHLA-DRA) acquires a different conformation, which in turn leads to its accumulation within the endoplasmic reticulum, where it is targeted for degradation. However, interactions with the peptide-binding pocket of canonical class II HLA molecules promote the translocation of sHLA-DRA to the cell surface and its partial protection from proteolysis. Lastly, we reported that immune cells from carriers of the allele coding for sHLA-DRA variant were characterized by a lower self-proliferation capacity, suggesting that distinct signaling pathways are activated by this intact neo-antigen [10].

Considering the potential biological impact of sHLA-DRA on the immune response, there are several questions that remained unanswered: first, the topography of binding of sHLA-DRA (lacking 25 residues from C-terminal) to the HLA-DR2 heterodimer. Second, consequential effect of this binding on functional properties of the complex. And third, whether the presence of a full-length protein like sHLA-DRA can spatially inhibit antigen presentation by HLA-DR2. To fill this knowledge gap, we characterized the structural determinants underlying this novel interaction in atomic resolution. By combining all-atom molecular dynamics (MD) simulations and *in vitro* assays, we show that the sHLA-DRA refolding process exposes a linear epitope in the α_2 domain, which interacts with the outer domain of the HLA peptide-binding groove. Moreover, despite no direct interaction with the HLA-DR2 peptide binding groove, we predict a significant structural impact of sHLA-DRA on the HLA binding pockets. To our knowledge, this is the most comprehensive study addressing the molecular geometry and underlying mechanisms of an intact antigen binding to class II HLA molecules.

Materials and Methods

Computational Methods

Structural modeling of sHLA-DRA—Molecular model of sHLA-DRA was constructed based on the structure of the long DRA isoform (PDB ID: 2Q6W) [10,22] using SWISS-MODEL [23]. Missing residues in sHLA-DRA mapped on the β-strands in the second immunoglobulin-like (Ig-like) domain of the long isoform and were replaced by a linker region connecting the first and second Ig-like domains. The linker was modeled based on a database of 700 million loops using the SuperLooper2 webserver [24]. The final structure of sHLA-DRA was solvated in the TIP3P explicit water model and minimized for 100,000 and equilibrated for 100 ns.

Docking of sHLA-DRA on the HLA heterodimer—Rigid docking between sHLA-DRA and HLA-DR2 was performed using the ZDOCK server version 3.0.2 [25,26]. It was first carried out without any residues selected or filtered out from sHLA-DRA, while surface residues on the first Ig-like domain of both HLA subunits were selected as the potential binding site on the receptor. Visual analysis of the top ten complexes (Supplementary Table S1) showed that a loop region in sHLA-DRA (residues R69 to G83) engaged most frequently with HLA-DR2, suggesting that it was an HLA binding site. The Z-dock

outcomes were scored based on Interface Atomic Contact Energies (IFACE) statistical potential, electrostatics, and shape complementarity terms.

We then performed flexible docking using HADDOCK on the top structure from the final docking step. Since the HLA binding groove is the most functionally important for high affinity antigen binding and presentation, we specified residues in this region within the 3 Å distance of the sHLA-DRA loop in the top-scored complex obtained from the rigid-docking stage as 'the active site'. All non-polar hydrogen atoms were removed. The ambiguous interaction restraints (AIRs) were partitioned in 2 and randomly excluded. HADDOCK first conducted rigid docking and produced 1000 structures, which were minimized. The best-scoring 200 structures were used for semi-flexible refinement. Fraction of common contact method was used for clustering the resulting complexes with a root-mean-square deviation (RMSD) cut-off of 0.6 Å. The electrostatic parameter was kept in both rigid and semi-flexible docking. Distance-dependent dielectric constant (ϵ) was 10 and 1 for rigid and semi-flexible docking, respectively. OPLSX parameters were used for non-bonded interactions and Kyte-Dolittle method was used for solvated docking. One solvation shell was generated and the water-surface-cutoff was set to 8 Å for solvated docking. The thickness of the water layer is determined according to the long-range electrostatic interactions between the protein and solvent. In the final analysis, the cut-off distance to define a hydrogen bond and a hydrophobic contact was 2.5 Å and 3.9 Å, respectively.

Molecular Dynamics Simulations—The best-scoring structure from the solvated docking was used to generate the initial configuration of the system. The sHLA-DRA molecule was moved from the HLA-DR2 surface such that a water layer could form between the molecules. The system was solvated with 150 mM KCl in a cell with box size of 17.2×12×9.1 nm^3, the final simulation cell consisted of 189,685 atoms. Point mutation were made using the Mutator plugin in Visual Molecular Dynamics (VMD) [27]. The NAMD package [28] and CHARMM36 force field [29] were used for all simulations. The cut-off of 1.2 nm and a switching function was used for van der Waals forces with a range of 1.0 nm. Particle Mesh Ewald was used for calculating electrostatic interactions with a grid spacing of 1 [30,31]. All simulations were conducted in the NPT ensemble at constant temperature of 310 K via Langevin dynamics with a damping coefficient of 5/ps only applied to non-hydrogen atoms. Pressure was maintained at 1 atm using Nose-Hoover Langevin piston pressure control with a barostat damping time scale of 50 fs. All hydrogen bonds were constrained using the LINCS algorithm [32]. The simulation time step was 2 fs. Simulations were run in triplicates for both wiltype and mutant proteins to achieve statistically significant information. The C_α atoms of C-terminal residues (D181 in the α-subunit and E193 in the β-subunit) of both HLA subunits were fixed to mimic membrane anchorage. All simulation trials ran for 240 ns using XSEDE computational resources [33]. Analysis was performed on all simulation frames spaced at 400 ps after removing the first 20 ns of data from each simulation repeat. Error bars were obtained from the standard error of mean over all simulation repeats. All visualization, energy, and distance calculations were performed using VMD [27]. Cross-correlation and normal model analyses were performed using the Bio3D package in R [34].

Free Energy of Binding—We employed Molecular Mechanics Poisson-Boltzmann Surface Area (MM-PBSA) approach to estimate binding affinities [19], which is appropriate for detecting large differences between HLA binding to the wildtype and mutant sHLA-DRA via $\Delta\Delta G = \Delta G_{Mut} - \Delta G_{WT} = \mathrm{RT}\ \ln(Kd_{Mut}/Kd_{WT})$. We used the CaFE package for the calculations [35]. The type of PB radii and boundary conditions were set to PARSE and multiple Debye- Huckel, respectively. Cubic B-spline was used to map charges to the grid. Surface area calculation was performed using 0.0054 kcal/mol $Å^2$ and 0.92 kcal/mol as surface tension and surface offset, respectively. Snapshots were taken from the last 20 ns of all simulation trajectories for the MM-PBSA calculations.

Pocket Volume and Area Calculations—Binding pocket volumes were computed using POVME3.0 [36]. The HLA binding groove from all frames of the MD trajectory was superimposed on the crystal structure of the peptide-loaded HLA heterodimer (PDB ID: 1BX2) [20]. Centers of spheres added to the pocket encompassing regions were then set to the centers of mass of side-chains of the $MBP_{85–99}$ peptide. The radius of regions was set to 7 Å to account for dynamic changes of the protein surface throughout the trajectory. A seed sphere was defined for each pocket centered at the big point field sphere but smaller radius (4 Å) to limit volume calculation to the contiguous pocket seed region and avoid including volume of other pockets covered by the larger pocket-encompassing point field. Two control simulations were carried out for pocket comparison, one with the $MBP_{85–99}$ loaded HLA (PDB ID: 1BX2) and one with the ligand-free HLA. Details of the simulations were consistent with the main simulations as described in the Molecular Dynamics Simulations section. One trajectory of 240 ns was generated for each control. The surface area of pockets are also computed by identifying a thin layer of volume lining the pocket and measuring the exposed surface.

Experimental Methods

Cell Lines—HeLa cells were obtained from the ATCC biobank and maintained in Dulbecco's modified Eagle's medium (GIBCO) supplemented with 10% v/v fetal bovine serum (GIBCO) at 37°C in a humidified atmosphere with 5% CO2.

Plasmids—The different pcDNA3.1 constructs containing the coding sequences for long and short HLA-DRA, and HLA-DRB1*15:01 have been described elsewhere [10]. The F76A mutation in sHLA-DRA construct was generated by site-directed mutagenesis using QuikChange Lightning Kit (Stratagene). The mutation was confirmed by Sanger sequencing.

In-cell enzyme-linked immunosorbent assay (ELISA)—The HLA-DRA molecule loading onto HLA molecules was evaluated by means of a robust in-cell ELISA assay we have previously optimized [10]. Briefly, HeLa cells were cultured in 12-well plates and transfected with different *HLA-DRA* constructs, either alone or in combination with *HLA-DRB1*15:01*, using Lipofectamine 2000 (Invitrogen). After 24 h, cells were reseeded in 96-well plates (80,000 cells/well) and cultured for additional 24 h. Cells were then fixed with 2% paraformaldehyde (PFA) for 10 min at RT, and blocked with 3% normal goat serum (NGS) in PBS for 1 h at RT. After one wash with PBS, cells were incubated with primary anti-HA (ab9110, Abcam) antibodies in 1% BSA solution (1:300) at 37°C

for 1 h. After three more washes, cells were incubated with horseradish peroxidase (HRP)-conjugated antibody (7074, Cell Signaling) in 1% bovine serum albumin (BSA) solution (1:2,500) at 37°C for 1 h. After three final washes, signals were developed using the 3,3′,5,5′-tetramethylbenzidine (TMB) substrate and absorbance values at 450 nm were detected with a Spectramax plate reader (Molecular Devices).

Western Blotting—HeLa cells were cultured in 12-well plates and transfected with different *HLA-DRA* constructs using Lipofectamine 2000 (Invitrogen). After 24 hours, cells were lysed in RIPA buffer (50 mM Tris–HCl, pH 7.5; 150 mM NaCl; 1% NP-40; 0.5% sodium deoxycholate, 0.2% sodium dodecyl sulphate) supplemented with protease inhibitors in tablets (Roche). Samples were separated by sodium dodecyl sulphate–polyacrylamide gel electrophoresis (SDS–PAGE) on 10% gels and then transferred to nitrocellulose membranes (Immobilion) at 100 V for 30 min. Membranes were then blocked with 5% milk in Tris-buffered saline supplemented with 0.05% Tween-20 (TBS-T) for 1 h at room temperature (RT) and then incubated with anti-HA (ab9110, Abcam) and anti-actin (8457, Cell Signaling) primary antibodies (1:1,000) in 5% bovine serum albumin (BSA) in TBST-T, overnight at 4°C. The next day, the membranes were washed three times with TBS-T and incubated with HRP-conjugated secondary antibodies (7074, Cell Signaling) in blocking solution (1:10,000) for 1 h at RT. After extensive washing in TBS-T, the chemiluminescent signals were detected with Supersignal West Dura reagent (Thermo Scientific), using a Molecular Imager ChemiDoc XRS System equipped with Quantity One software (Bio-Rad).

Statistical Analyses

Data presented in this study come from three independent MD runs and/or experiments and is presented as mean ± SEM. Differences between multiple groups were estimated using ANOVA and between means of two groups were assessed with two-tailed Student's t-test. Corrected P-values were obtained using Bonferroni's formula and were considered significant when $< 0.05/n$, where n is the number of tests.

Results and Discussion

To determine the binding site on sHLA-DRA, we performed rigid docking followed by flexible docking between sHLA-DRA and the peptide-free HLA-DR2 molecule composed of α and β chains encoded by *HLA-DRA* and *HLA-DRB1*15:01* alleles, respectively. The sHLA-DRA molecule conforms to a distinct fold compared to the long isoform, resulting in the exposure of a loop region between residues 69 to 83 ($LR_{69–83}$) [10]. The $LR_{69–83}$ region was invovled in the HLA interaction in seven out of ten predicted complexes (Fig. 1a–b). The best-scoring complex in flexible docking was then used to generate the initial configuration of the system in which sHLA-DRA was displaced along HLA-DR2 axis allowing water layers to form on both molecular surfaces before the system was equilibrated for 240 ns in three independent MD runs (Fig. 1c).

The sHLA-DRA molecule formed both transient and stable interactions with HLA-DR2 throughout the simulation time. Interaction energies per residue of sHLA-DRA confirmed that only the $LR_{69–83}$ region was consistently engaged with the HLA-DR2 surface (Fig. 2a). The N-terminal residues of sHLA-DRA formed weak transient interactions, which are likely

an artifact of floppiness of this region and not critical for molecular anchorage. The heatmap of nonbonded interaction energies of $LR_{69–83}$ in Fig. 2a suggests that R75, E72, and F76 are three key residues for HLA association, from strongest to weakest. Nonetheless, the contact index of these residues with HLA, defined as the number of HLA atoms within 3 Å from these residues, confirmed that F76 had the highest contact surface both in the beginning and throughout the simulation repeats, followed by R75 and E72. The higher nonbonded energies of E72 and R75 in Fig. 2b are due to the stronger contribution of electrostatic interactions, however F76 plays a key role in the initial anchorage of sHLA-DRA to the HLA molecule. Specifically, a cation-π interaction between F76 on sHLA-DRA and R76 on the HLA-DR2 α-chain mediated both initial engagement and stable interaction in the first binding mode as shown in Supplementary Fig. 1a. Although this interaction was transient in the second binding mode, it was still important for early surface engagement. Both repulsive and attractive forces exerted by R55 in the HLA-DR2 β-chain on F76 guided the final conformation of the second binding mode (Supplementary Fig. 1b). Mutating E72 and R75 to alanine in two separate simulations demonstrated that F76 was indeed sufficient to anchor sHLA-DRA to HLA-DR2 as shown in Supplementary Fig. 2.

Our simulations showed a dynamic binding between sHLA-DRA and HLA resulting in semi-stable interactions of sHLA-DRA with different sites outside the binding groove. However, in none of the simulations was sHLA-DRA directly associated with the peptide binding pockets inside the groove. One stable binding mode of sHLA-DRA was near the 11^{th} pocket but further towards the end of the groove (Fig. 2c), mediated by F76 and R75 on sHLA-DRA interacting with R76 on the α-chain and P56 and E52 on the β-chain. While all three simulations started from the same initial configuration, in two out of three runs, sHLA-DRA diffused away from the initial position towards the side of HLA-DR2, characterized by the distance between F76 on sHLA-DRA and R76 on HLA-DR2 (Supplementary Fig. 3). In this binding mode, sHLA- DRA engaged with the outer region of the groove on the β-chain (Fig. 2d–e). Interestingly, the R75A and E72A mutations on sHLA-DRA promoted the first and second binding modes, respectively (Supplementary Fig. 2). These observations are also in agreement with previous experimental data showing that co-immunoprecipitation of long and short HLA-DRA chains takes place only when the β-chain is present in the system [10]. Interestingly, this dominant binding mode is somehow reminiscent of the interactions taking place between superantigens (SAgs) and class II molecules [11]. SAgs are particular toxins of bacterial or viral origin that are able to elicit a massive T cell activation as compared to traditional antigens [12,13]. SAgs bind to the outer region of the groove—more frequently on the α-chain, but also at the level of the β-chain through a zinc ion [14–16]. Although we cannot formally attribute the SAg status to sHLA-DRA, such structural analogies might be indicative of evolutionary intersections with this class of antigens. In line with this scenario, at least one other intact antigen - the class I allotype HLA-Cw4- has been shown to efficiently trigger the activation of B cells [9].

Furthermore, we have presented evidence suggesting that sHLA-DRA expression might affect the proliferation of specific immune cell populations [10]. Remarkably, the $LR_{69–83}$ region identified in this study as the HLA-DRB ‘binding site’ in sHLA-DRA overlaps with the HLA-DRA-derived self-peptides (residues 70 to 85) eluted from HLA-DR2 molecules (Supplementary Table 2), which have been suggested to mediate altered autologous T cell

proliferation in the context of multiple sclerosis [17], further corroborating the biological importance of the $LR_{69–83}$ epitope in the HLA-DRA chain.

The interactions between intact antigens and HLA molecules are likely rare biological events, thereby full-length proteins have had limited exposure to HLA binding throughout their evolution. Since mutual binding sites have not co-evolved for high affinity interactions, multiple binding modes of the intact protein with different regions of HLA might exist. These binding modes can have distinct configurations and may have overlapping contact surfaces on either of the binding partners. In our study, the binding site on sHLA-DRA remained the same in both binding modes (Fig. 2d–2e), while two binding surfaces were predicted on the HLA molecule. It is important to note, however, that the strong linkage disequilibrium between the variant promoting the short isoform and specific DRB1 allotypes including DRB1*15:01 likely suggests related functionalities that are not yet understood.

The simulation results strongly suggest that F76 on sHLA-DRA plays a critical role in mediating the binding between sHLA-DRA and the HLA-DR2 heterodimer. To further validate this key prediction, we first generated a structural model of sHLA-DRA in which an alanine residue substituted the phenylalanine at position 76 (F76A point mutation). This change is expected to eliminate key cation-π interactions [18] between F76 and basic residues mediating both binding modes. Using the same initial configuration as the wildtype, we monitored the binding between the mutant sHLA-DRA and HLA–DR2 in 120 ns of simulation. Interestingly, within 20 ns of simulation time, the F76A mutant diffused away from the HLA-DR2 surface failing to form any stable interactions (Fig. 3a–3b). This result confirmed the importance of the long F76 side-chain in anchoring sHLA-DRA to the HLA molecule. Indeed, weak interactions between E72 and R75 were not sufficient to stabilize the molecule. The MM-PBSA method [19] was used to estimate the free energy of binding between HLA-DR2 and both wildtype and F76A mutant sHLA-DRA. The free energy change ($\Delta\Delta G$) of +5.2 kcal/mol upon the F76A mutation was observed. However meaningful, it should be noted that this method provides an approximation of the real binding affinities, which are shown to be overestimated. For this reason, we experimentally validated the *in silico* results by employing a validated in-cell ELISA assay optimized to demonstrate the cell surface exposure of sHLA-DRA upon interaction with the standard HLA molecule. In this setup, the HLA heterodimer was co-expressed in HeLa cells along with an HA-tagged version of sHLA-DRA, either wildtype or bearing the F76A mutation (Fig. 3c). The quantification of sHLA-DRA on the cell surface by HA staining highlighted significantly lower levels of the F76A mutant as compared to the wildtype protein. Importantly, the decreased levels of the mutant were not due to its impaired expression as confirmed by Western blotting (Fig. 3d). Altogether, these data were consistent with the molecular simulations and support the fundamental function of the F76 residue in stabilizing the interaction with the HLA heterodimer.

Despite no direct binding to the HLA peptide groove, sHLA-DRA still modulated peptide binding pockets through allosteric effects on the protein structure. In detail, volumes and exposed surfaces of all antigen binding pockets of HLA-DR2 in complex with sHLA-DRA were quantified and compared with two additional states of HLA-DR2: one bound to the $MBP_{85–99}$ peptide [20] and as a reference, one in the ligand-free state. There are 14 peptide

binding pockets along the HLA binding groove (Fig. 4a). The binding of sHLA-DRA affected most HLA-DR2 pocket volumes such that the volume distributions resembled those of the MBP-bound HLA-DR2 (Fig. 4a). Specifically, pocket volumes of P-2 to P1, P4 to P7, and P9 were not statistically different from those in the ligand-bound HLA ($P > 0.05/2$, Bonferroni corrected for two tests, Supplementary Table S3), whereas P10 and P11 were most statistically deviated ($P < 0.002$). Pockets P1, P4, P6, and P9 that collectively determine specificity of the anchor peptide residues binding to MHC class II isotypes [21] were among the pockets with a more stable volume. It is important to note that in these simulations, variations in the pocket volumes were allosterically regulated through one-sided interaction of sHLA-DRA with the HLA β-chain without $MBP_{85–99}$ being loaded in the HLA binding groove. Interestingly, the average size of binding pockets in the N-terminal end of the binding groove (P-3 to P-1) was reduced by both the $MBP_{85–99}$ peptide and sHLA-DRA, while other pockets were enlarged upon binding. This suggests that initial anchorage of $MPB_{85–99}$ peptide to the N-terminal end are likely facilitated by relatively open pockets. The middle pockets are relatively larger to accommodate deeper interactions of long and branched side-chains. Overall, a plausible proportion of variations in pocket volumes were similarly modulated by direct interaction of $MBP_{85–99}$ peptide and sHLA-DRA. To further demonstrate allosteric regulation of the HLA-DR2 structure, a cross-correlation analysis (CCA) was performed on all three binding simulations between the sHLA-DRA and HLA-DR2 as well as HLA-DR2 with and without the $MBP_{85–99}$ ligand. The CCA analysis quantifies the level by which atomic fluctuations of different parts of the protein structure are correlated with one another throughout the simulation trajectories. This analysis indicated that atomic correlations in the β-chain of HLA-DR2 is much stronger in the bound state of the molecule to both sHLA-DRA and the $MBP_{85–99}$ ligand relative to the ligand-free HLA-DR2, indicating that both proximal and distal regions of the chain are affected by local interactions of either $MBP_{85–99}$ or sHLA-DRA as shown in Supplementary Fig. 4. Such correlations were not observed in the α-chain. Furthermore, normal mode analysis (NMA) was performed on the equilibrated HLA-DR2 structure isolated from the last frame of the ligand-bound and control simulations to assess structural flexibility (Supplementary Fig. 5). Consistent with the CCA analysis, there was no significant difference in the level of atomic fluctuations of the HLA-DR2 α-chain after being subjected to sHLA-DRA/$MPB_{85–99}$ binding compared to its ligand-free state (Supplementary Fig. 5a). On the contrary, atomic fluctuations of residues 107 to 116, mapping to the β_2 domain of HLA-DR2, were significantly reduced upon the sHLA-DRA/MBP association compared to the ligand-free state. Specifically, the first sHLA-DRA binding mode (sHLA-DRA-bound Run 2 in Supplementary Fig. 5b) decreased fluctuations of this region in a similar fashion as the $MBP_{85–99}$ peptide; whereas lower level of fluctuations in this region was induced by the second sHLA-DRA binding mode (sHLA-DRA-bound Run 1 and 3 in Supplementary Fig. 5c). The proximity of the affected region in the β_2 domain to the lipid membrane suggests that sHLA-DRA/peptide binding alters signal transmission towards the lipid membrane.

The surface areas of pockets showed less significant changes across the simulations as compared to the pocket volumes (Fig. 4c and Supplementary Table S4). The most significant change was in P-2 relative to the ligand-free HLA-DR2. The sHLA-DRA isoform effect on the surface areas of P3 and P4 was different from $MBP_{85–99}$ peptide, while surface areas of

pockets P-3 to P-1, P2, P5, and P8 were changed compared to the ligand-free HLA-DR2. Notably, the largest pocket P5 showed a decrease in the volume, but an increase in the surface area, suggesting a shape change at the center of the groove. It has previously been shown that the HLA class II pockets can accommodate large aromatic side-chains, e.g. in tyrosine or phenylalanine, while class I pockets are too shallow for such interactions [4,7]. Thus, changing the pocket size may profoundly affect epitope selectivity and loading of class II molecules.

In summary, by combining detailed molecular simulations with *in vitro* assays, we reveal for the first time the structural basis of the interaction between an alternative splicing isoform of HLA-DRA and classical class II HLA molecules. Our results suggest at least three possible mechanisms through which sHLA-DRA expression may affect the immune response: 1) structural modification of the peptide binding pocket, modulating epitope selectivity and loading; 2) imposition of steric hindrance for T cell receptor (TCR) association; and 3) serving as a neo-antigen presented by HLA. To discriminate between these hypotheses, it would be important to verify whether short peptides can still be efficiently presented when sHLA-DRA is bound onto the HLA molecule. In our previous study, we have shown that co-expression of the invariant chain (Ii) abolishes sHLA-DRA binding, suggesting that they compete for binding to the peptide binding groove. Nevertheless, it should be noted that full-length Ii is a trimer that imposes a considerable steric hindrance around the HLA binding groove including the outer region, and thus can eliminate any association of other bulky proteins. These findings will motivate further studies involving professional antigen-presenting cells (APCs) with the ability to process the invariant chain and leave only the CLIP peptide associated in order to address the possible immunomodulatory function of sHLA-DRA.

Supplementary Material

Refer to Web version on PubMed Central for supplementary material.

Acknowledgements

The work was supported by the National Institutes of Health (R01NS102153). This work used the Extreme Science and Engineering Discovery Environment (XSEDE) resource-name at the service-provider through allocation MCB200213. The study was also supported by FISM-Fondazione Italiana Sclerosi Multipla Senior Research Fellowships Cod. 2014/B/1 and Cod. 2017/B/3 co-financed with the “5 per mille” public funding. HS is a postdoctoral fellow of the National Multiple Sclerosis Society (FG-1807-31603). This publication was also supported by the National Center for Advancing Translational Sciences, National Institutes of Health, through UCSF-CTSI Grant Number TL1 TR001871 to HS.

Data availability

This study includes no data deposited in external repositories. All the data supporting the findings of this study are available from the corresponding author upon reasonable request.

References

[1]. Kulski JK, Shiina T, Anzai T, Kohara S, Inoko H, Comparative genomic analysis of the MHC: the evolution of class I duplication blocks, diversity and complexity from shark to man, Immunol. Rev 190 (2002) 95–122. [PubMed: 12493009]

[2]. Neefjes J, Jongsma MLM, Paul P, Bakke O, Towards a systems understanding of MHC class I and MHC class II antigen presentation, Nat. Rev. Immunol 11 (2011) 823–836. [PubMed: 22076556]

[3]. McCluskey J, Peh C, The human leucocyte antigens and clinical medicine: an overview, Rev Immunogenet. 1 (1999) 3–20. [PubMed: 11256570]

[4]. Stern LJ, Brown JH, Jardetzky TS, Gorgat JC, Urban RG, Strominger JL, Wiley DC, Crystal structure of the human class II MHC protein HLA-DR1 complexed with an influenza virus peptide, Nature. 368 (1994) 215–221. [PubMed: 8145819]

[5]. Madden DR, Gorga JC, Strominger JL, Wiley DC, The three-dimensional structure of HLA-B27 at 2.1 A resolution suggests a general mechanism for tight peptide binding to MHC, Cell. 70 (1992) 1035–1048. [PubMed: 1525820]

[6]. Williams TM, Human leukocyte antigen gene polymorphism and the histocompatibility laboratory, J. Mol. Diagnostics 3 (2001) 98–104.

[7]. Runnels HA, Weber DA, Moore JC, Westerman LE, Jensen PE, Intact proteins can bind to class II histocompatibility molecules with high affinity, Mol. Immunol 34 (1997) 471–480. [PubMed: 9307063]

[8]. Lindner R, Unanue ER, Distinct antigen MHC class II complexes generated by separate processing pathways, EMBO J. 15 (1996) 6910–6920. [PubMed: 9003767]

[9]. Jiang Y, Arase N, Kohyama M, Hirayasu K, Suenaga T, Jin H, Matsumoto M, Shida K, Lanier LL, Saito T, Arase H, Transport of misfolded endoplasmic reticulum proteins to the cell surface by MHC class II molecules, Int. Immunol 25 (2013) 235–246. [PubMed: 23334921]

[10]. Didonna A, Damotte V, Shams H, Matsunaga A, Caillier SJ, Dandekar R, Misra MK, Mofrad MRK, Oksenberg JR, Hollenbach JA, A splice acceptor variant in HLA-DRA affects the conformation and cellular localization of the class II DR alpha-chain, Immunology. 162 (2021) 194–207. [PubMed: 32986852]

[11]. Jardetzky TS, Brown JH, Gorga JC, Stern LJ, Urban RG, Chi Y, Stauffacher C, Strominger JL, Wiley DC, Three-dimensional structure of a human class II histocompatibility molecule complexed with superantigen, Nature. 368 (1994) 711–718. [PubMed: 8152483]

[12]. Herman A, Kappler JW, Marrack P, Pullen AM, Superantigens: mechanism of T-cell stimulation and role in immune responses, Annu. Rev. Immunol 9 (1991) 745–772. [PubMed: 1832875]

[13]. Llewelyn M, Cohen J, Superantigens: microbial agents that corrupt immunity, Lancet Infect. Dis 2 (2002) 156–162. [PubMed: 11944185]

[14]. Fraser JD, Hudson KR, Superantigens-remnants of a past process?, Res. Immunol 144 (1993) 188–193. [PubMed: 7694344]

[15]. Sundberg EJ, Deng L, Mariuzza RA, TCR recognition of peptide/MHC class II complexes and superantigens, Semin Immunol. 19 (2007) 262–271. 10.1016/j.smim.2007.04.006.TCR. [PubMed: 17560120]

[16]. Kim J, Urban R, Strominger J, Wiley D, Toxic shock syndrome toxin-1 complexed with a class II major histocompatibility molecule HLA-DR1, Science (80-.) 266 (1994) 1870–1874.

[17]. Mohme M, Hotz C, Stevanovic S, Binder T, Lee J, Okoniewski M, Eiermann T, Sospedra M, Rammensee H, Martin R, HLA-DR15-derived self-peptides are involved in increased autologous T cell proliferation in multiple sclerosis, Brain. 136 (2013) 1783–1798. [PubMed: 23739916]

[18]. Gallivan JP, Dougherty DA, Cation-pi interactions in structural biology, Proc. Natl. Acad. Sci 96 (1999) 9459–9464. [PubMed: 10449714]

[19]. Wang C, Nguyen PH, Pham K, Huynh D, Le T-BN, Wang H, Ren P, Luo R, Calculating protein-ligand binding affinities with MMPBSA: Method and error analysis, J. Comput. Chem 37 (2016) 2436–2446. 10.1002/jcc.24467. [PubMed: 27510546]

[20]. Smith BKJ, Pyrdol J, Gauthier L, Wiley DC, Wucherpfennig KW, Crystal structure of HLA-DR2 (DRA*0101, DRB1*1501) complexed with a peptide from human myelin basic protein, J. Exp. Med 188 (1998) 1511–1520. [PubMed: 9782128]

[21]. Jones EY, Fugger L, Strominger JL, Siebold C, MHC class II proteins and disease: a structural perspective, Nat. Rev. Immunol 6 (2006) 271–282. [PubMed: 16557259]

[22]. Parry CS, Gorski J, Stern LJ, Crystallographic structure of the human leukocyte antigen DRA, DRB3*0101: models of a directional alloimmune response and autoimmunity, J. Mol. Biol 371 (2007) 435–446. [PubMed: 17583734]

[23]. Waterhouse A, Bertoni M, Bienert S, Studer G, Tauriello G, Gumienny R, Heer FT, de Beer TAP, Rempfer C, Bordoli L, Lepore R, Schwede T, SWISS-MODEL: homology modelling of protein structures and complexes, Nucleic Acids Res. 46 (2018) 296–303. 10.1093/nar/gky427.

[24]. Ismer J, Rose AS, Tiemann JKS, Goede A, Preissner R, Hildebrand PW, SL2: an interactive webtool for modeling of missing segments in proteins, Nucleic Acids Res. 44 (2016) W390–W394. [PubMed: 27105847]

[25]. Pierce BG, Hourai Y, Weng Z, Accelerating protein docking in ZDOCK using an advanced 3D convolution library, PLoS One. 6 (2011) 1–6.

[26]. Mintseris J, Pierce B, Wiehe K, Anderson R, Chen R, Weng Z, Integrating statistical pair potentials into protein complex prediction, Proteins. 69 (2007) 511–520. [PubMed: 17623839]

[27]. Humphrey W, Dalke A, Schulten K, VMD: Visual molecular dynamics, J. Mol. Graph 14 (1996) 33–38. [PubMed: 8744570]

[28]. Phillips JC, Hardy DJ, Maia JDC, Stone JE, V Ribeiro J, Bernardi RC, Buck R, Fiorin G, Henin J, Jiang W, McGreevy R, Melo MCR, Radak BK, Skeel RD, Singharoy A, Wang Y, Roux B, Aksimentiev A, Luthey-Schulten Z, V Kale L, Schulten K, Chipot C, Tajkhorshid E, Scalable molecular dynamics on CPU and GPU architectures with NAMD, J. Chem. Phys 153 (2020) 044130. [PubMed: 32752662]

[29]. Huang J, MacKerell ADJ, CHARMM36 all-atom additive protein force field: Validation based on comparison to NMR data, J. Comput. Chem 34 (2013) 2135–2145. [PubMed: 23832629]

[30]. Darden T, York D, Pedersen L, Particle mesh Ewald: An N.log(N) method for Ewald sums in large systems, J. Chem. Phys 98 (1993) 10089.

[31]. Essmann U, Perera L, Berkowitz ML, A smooth particle mesh Ewald method, J. Chem. Phys 103 (1995) 8577.

[32]. Hess B, P-LINCS : a parallel linear constraint solver for molecular simulation, J. Chem. Theory Comput 4 (2008) 116–122. [PubMed: 26619985]

[33]. Towns J, Cockerill T, Dahan M, Foster I, Gaither K, Grimshaw A, Hazlewood V, Lathrop S, Lifka D, Peterson GD, Roskies R, Scott JR, Wilkins-Diehr N, XSEDE: Accelerating Scientific Discovery, Comput. Sci. Eng 16 (2014) 62–74.

[34]. Grant BJ, Rodrigues APC, ElSawy KM, McCammon JA, Caves LSD, Bio3d : an R package for the comparative analysis of protein structures, Bioinformatics. 22 (2006) 2695–2696. 10.1093/bioinformatics/btl461. [PubMed: 16940322]

[35]. Liu H, Hou T, CaFE: a tool for binding affinity prediction using end-point free energy methods, Bioinformatics. 32 (2016) 2216–2218. [PubMed: 27153651]

[36]. Wagner JR, Sørensen J, Hensley N, Wong C, Zhu C, Perison T, Amaro RE, POVME 3.0: software for mapping binding pocket flexibility, J. Chem. Theory Comput 13 (2017) 4584–4592. [PubMed: 28800393]

- A spicing acceptor variant drives the expression of a shorter isoform of HLA-DRA.
- Short HLA-DRA binds the outer domain of peptide-binding pockets in canonical HLA.
- A linear epitope that is exposed in short HLA-DRA mediates this interaction.
- Short HLA-DRA allosterically alters the pocket conformation upon binding HLA.

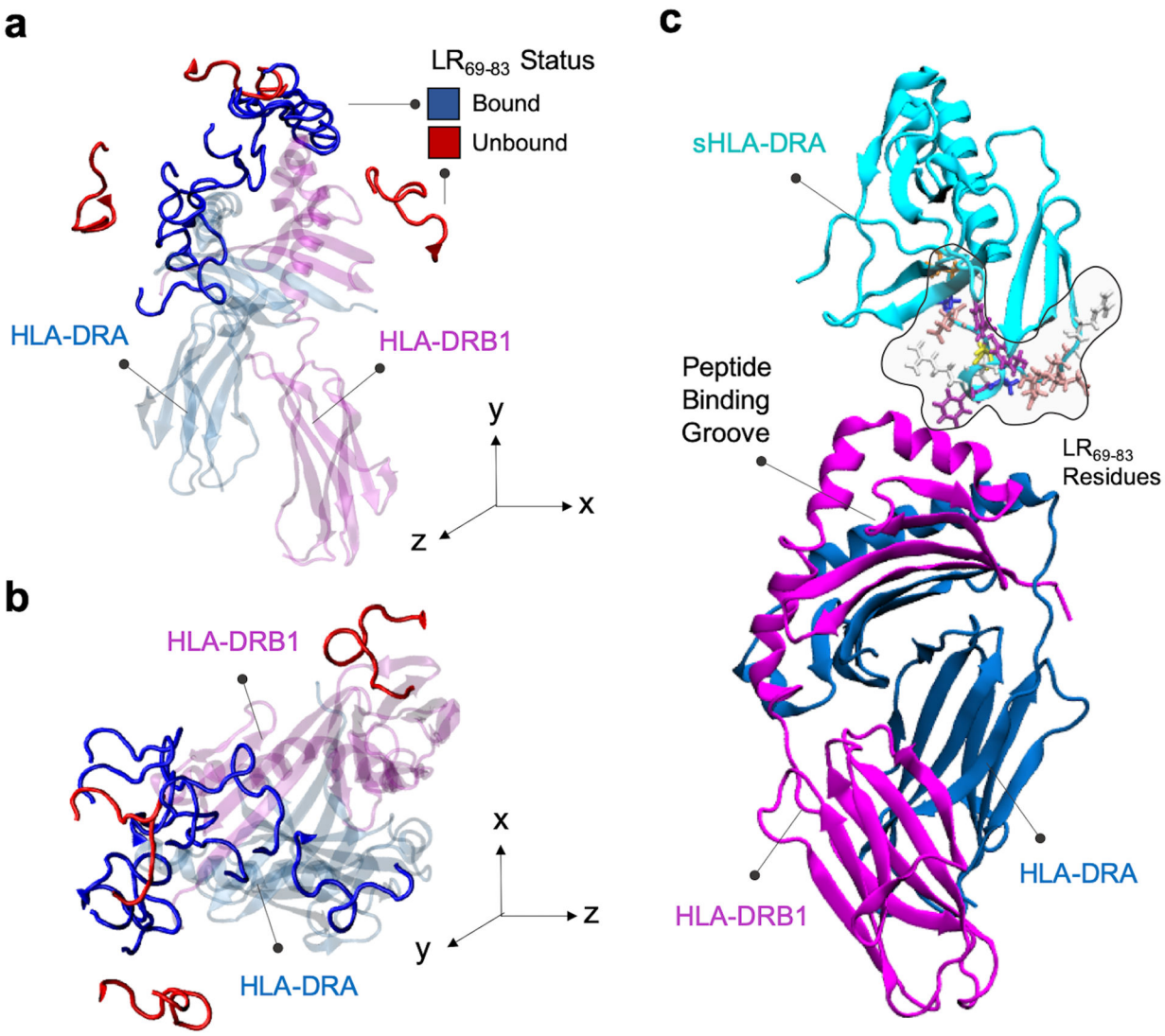

Figure 1 - The initial configuration of the system comprising sHLA-DRA and the HLA heterodimer.

a) Rigid docking predicted the association of the $LR_{69–83}$ loop in sHLA-DRA with HLA-DR2 in 70% of the top ten complexes. Only the $LR_{69–83}$ loop in sHLA-DRA is displayed for clarity. The $LR_{69–83}$ loop is colored based on its status in each predicted complex, i.e. associated with (blue) or dissociated from (red) the HLA-DR2 surface. **b)** The top view of the top ten complexes shown in **a**. **c)** The best-scoring complex from the solvated flexible docking was used to generate the initial configuration of the system. Side-chains of $LR_{69–83}$ are shown in the ball-and-stick representation.

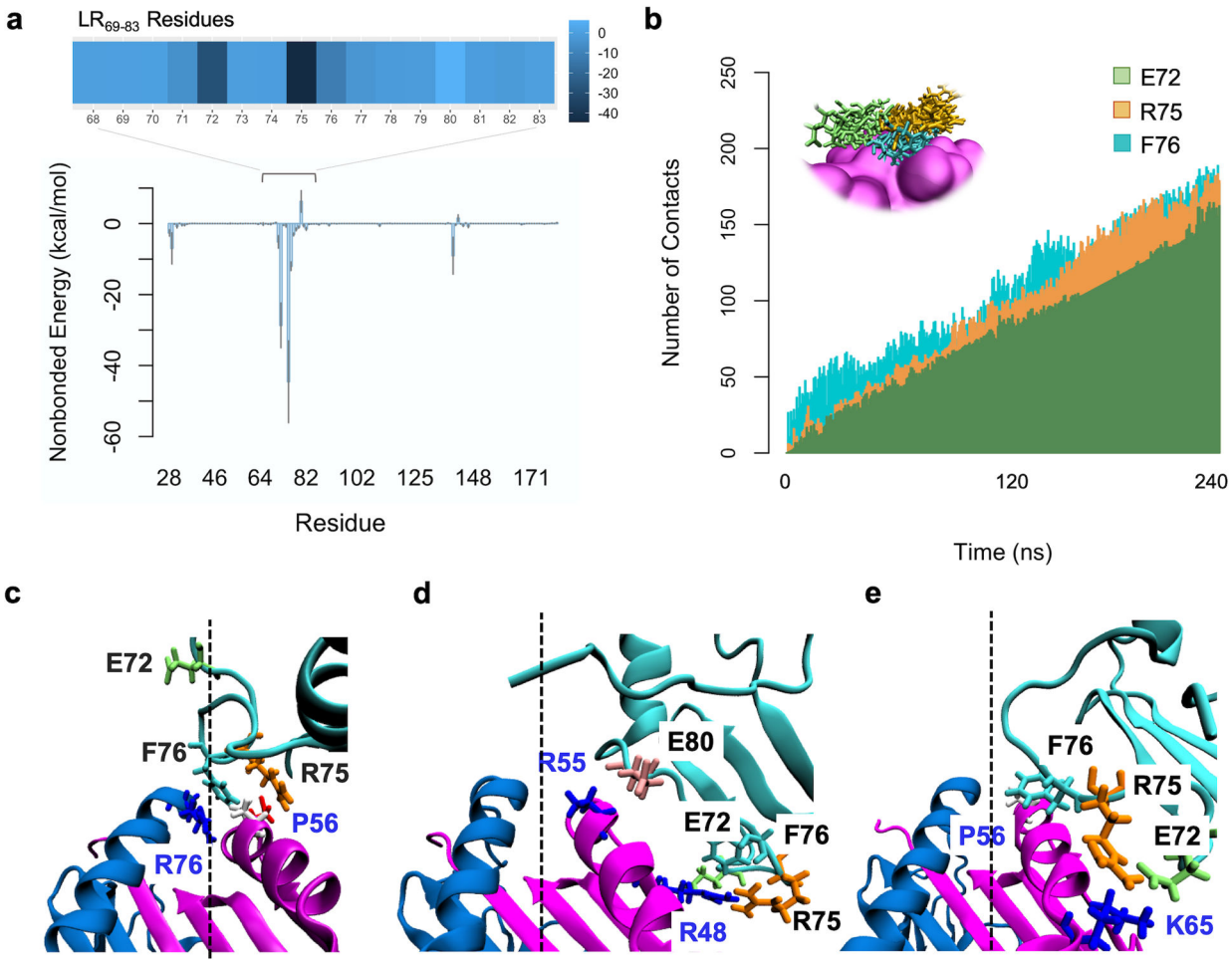

Figure 2 - Two distinct binding modes of sHLA-DRA and HLA-DR2.

a) The nonbonded interaction energy per residue of sHLA-DRA indicated that only the loop region of this molecule strongly associated with HLA-DR2. Standard error bars were computed for the three simulation trials. The heatmap showing the interaction energy of the sHLA- DRA loop region highlights the importance of residues 72, 75, and 76 in HLA-DR2 association. **b)** Number of contacts at each time step was quantified as the number of HLA-DR2 atoms within 3 Å distance of residues 72, 75, and 76 of sHLA-DRA. **c, d, e)** shows two distinct modes of sHLA-DRA binding to HLA-DR2. sHLA-DR2 associated with both HLA-DR2 subunits and remained stable throughout the simulation in the first shown binding mode captured in one simulation trial (**c**). **d**, **e)** shows the sHLA-DRA associated only with the outer region of the β-chain, which occurred in two simulation trials. The sHLA-DRA and HLA-DR2 residues are shown in black and royal blue, respectively. The dashed line marks the middle axis of the HLA peptide-binding groove.

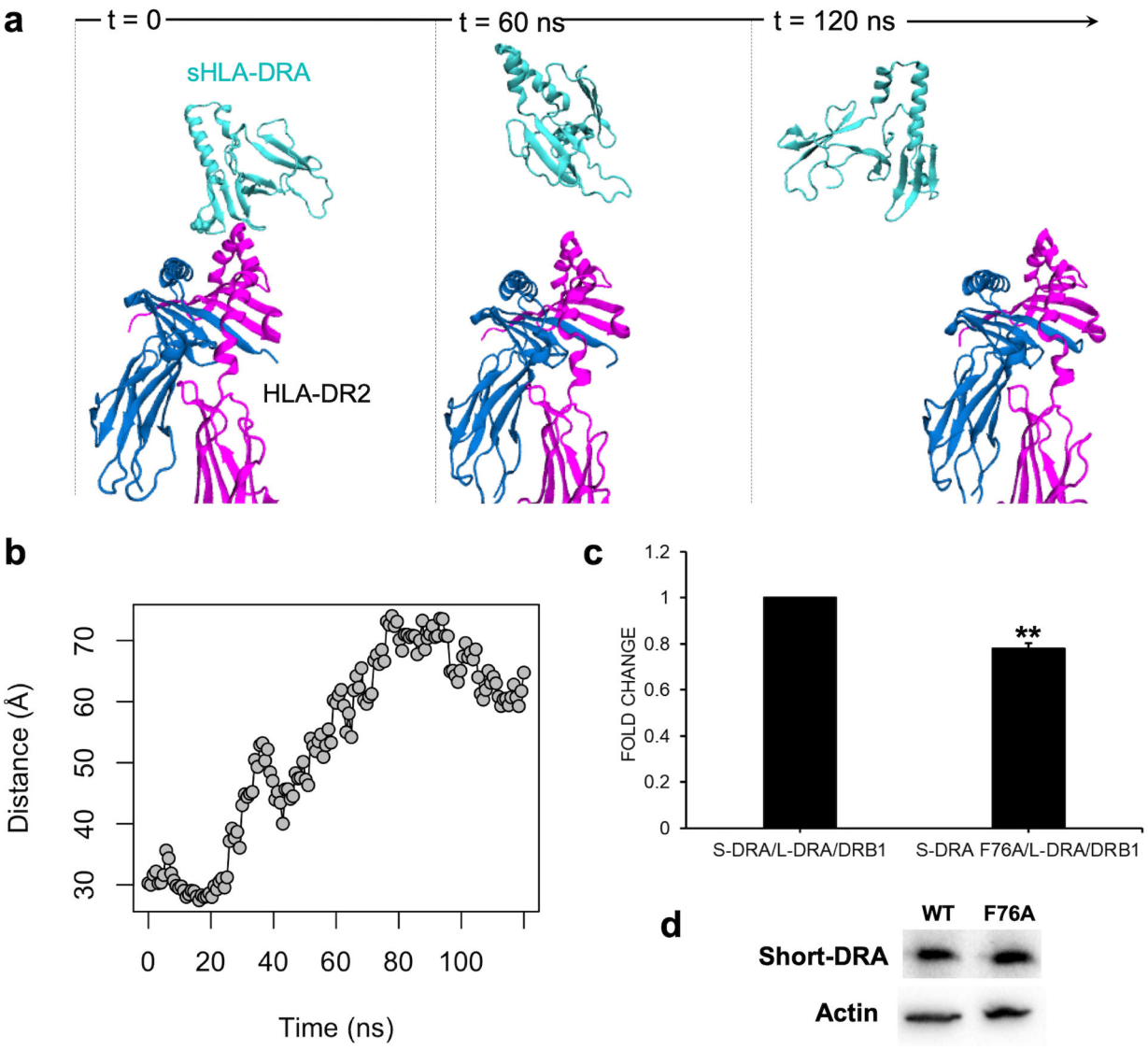

Figure 3 - The key role of F76 in mediating the HLA-DR2 association.

a) depicts sHLA-DRA molecule diffusing away from the HLA-DR2 surface in the F76A mutant using different time frames shown in the left, middle and right panels. **b)** The distance between the center of masses of mutant sHLA-DRA and HLA-DR2 is shown. **c)** The surface exposure of sHLA-DRA, wildtype and F76A mutant, in HeLa cells expressing the canonical HLA heterodimers was quantified by ELISA (as described in the Methods section). The levels of the F76A mutant were significantly lower compared to the wildtype molecule as shown in the bar chart (**$P \leq 0.01$). **d)** HeLa cells transfected with either sHLA-DRA or the F76A mutant were tested by Western blotting, using an antibody against their HA tag. Actin levels served as loading controls.

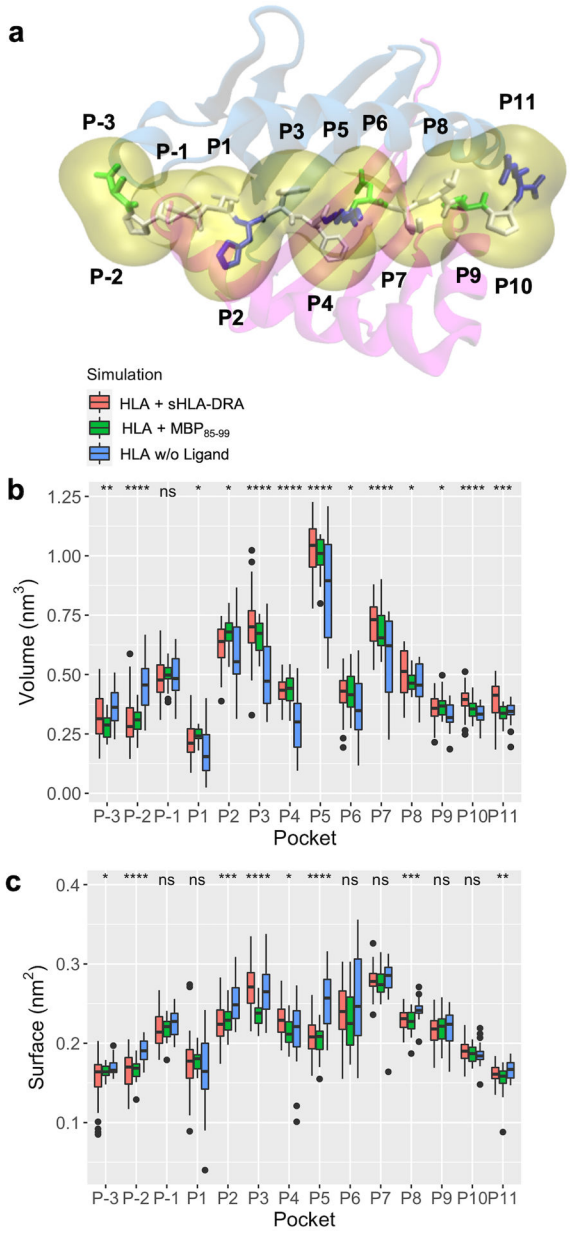

Figure 4 - The sHLA-DRA molecule allosterically modulates the peptide-binding pockets of HLA-DR2.

a) Binding pockets along the peptide binding groove of HLA-DR2. **b)** Distributions of peptide binding pocket volumes of HLA-DR2 interacting either with the sHLA-DRA (red), $MBP_{85–99}$ peptide (green), or ligand-free state labeled as W/O Ligand (blue). The sHLA-DRA isoform and MBP peptide induced similar fluctuations in most pocket volumes. **c)** Surface areas of the binding pockets demonstrated less significant changes in response to presence and type of the HLA ligand. The significance levels shown above the boxplots are ANOVA tests per pocket, * $P < 0.05$, ** $P < 0.005$, *** $P < 0.0005$, **** $P < 0.00005$, and ns stands for non-significant.